

Heat Transfer Analysis in Reiner–Philippoff Fluid via Finite Element Approach

N. JABBAR^{a,*}, W. SUMELKA^a AND U. NAZIR^b

^a*Institute of Structural Analysis, Poznan University of Technology, 61-138 Poznań, Poland*

^b*Department of Mathematics, Faculty of Science, KhonKaen University, KhonKaen 40002, Thailand*

Received: 01.11.2023 & Accepted: 20.02.2024

Doi: [10.12693/APhysPolA.145.256](https://doi.org/10.12693/APhysPolA.145.256) *e-mail: noman.jabbar@doctorate.put.poznan.pl

In this article, we discuss the increase in Reiner–Philippoff liquid thermal energy and mass transfer through a perpendicular plane in the presence of the magnetizing field. Characterizations regarding mass dissipation and heat energy are improved using non-Fourier’s analysis with the existence of a thermal source. Three kinds of nanoparticles, i.e., titanium dioxide, silicon dioxide, and aluminum oxide, are introduced in engine lubricants to create thermal energy. Darcy–Forchheimer analysis is adopted to examine the effects of flow and thermal energy. Furthermore, the Dufour and Soret effects are also discussed. A developing model is converted into a system of ordinary differential equations using similarity variables and solved using the finite element method. It is observed that the heat energy of the fluid increased as opposed to a higher rate of time relaxation number. Moreover, the fluid concentration declined as opposed to changes in the Schmidt number and chemical reaction parameters.

topics: porous media, non-Newtonian fluid, Cattaneo–Christov heat flux model, heat source

1. Introduction

The most significant applications related to nanofluids are of substantial interest in science and engineering. Nanotechnology applications are perceived as modern science that attracts researchers to study models based on nanofluids, including their various aspects. Nanofluids are defined as a combination of nanoparticles, including a base fluid. Ali et al. [1] developed a model concerning hybrid nanofluid in the presence of magnetic field-inserted slip conditions involving Jeffrey material. Ali et al. [2] investigated the enhancement of heat energy in the occupancy of viscous dissipation, utilizing a hybrid nanofluid approach. Ahmed et al. [3] used a numerical method to determine the numeric influences of thermal transfer in the existence of nanoparticles with fluctuating viscosity in heated channels. The impact of a magnetizing field on the thermal properties of nanofluids, including chemical reactions and viscous dissipation of heat, was investigated by Gopal et al. [4]. Moreover, Oke et al. [5] studied thermal characteristics utilizing nanoparticles in the presence of a thermal source and the inertial force in water. Saleem et al. [6] studied nanoparticles’ thermal properties and energy in a heated wavy medium. Next, Elnaqeeb et al. [7] investigated how to improve the transfer of heat using tri-hybrid nanoparticles in three-dimensional flows with water as the base fluid and different patterns of water. Hou et al. [8] studied the energy characteristics of

pseudo-plastic materials with tri-hybrid nanoparticles utilizing the finite element technique. They developed the idea that tri-hybrid nanoparticles gain the most heat. Also, Wang et al. [9] utilized the finite element approach to analyze the transport of mass and heat including tri-hybrid nanoparticles in ethylene glycol on a stretching surface. The finite element method (FEM) was also applied by Nazir et al. [10] to represent hybrid nanoparticles in the rheology of a hyperbolic tangent above a stretching plane. Manjunatha et al. [11] have investigated the ternary nanofluid effects on convective heat transfer over a heated surface. They used the shooting method to obtain numerical findings. Adun et al. [12] investigated energy enhancement in the presence of a mixture of three forms of nanoparticles using thermophysical properties.

It is important to emphasize that the classic case of Fourier’s law reveals the standard energy transfer process. One notable drawback of the parabolic heat energy equation is that the system’s answer is observed instantly in the whole medium. In this context, the need for non-Fourier law is clear for complex materials and can be considered an extension of Fourier’s law based on thermal relaxation time.

Nazir et al. [13] analyzed energy transfer effects in the Carreau fluid utilizing Cattaneo–Christov simulation over a stretching surface. To account for the presence of changing viscosity, they used finite elements. Nazir et al. [14] utilized the non-Fourier’s

Nomenclature. TABLE I

Symbol	Name
B_0	magnetic field value
Q_0	heat source
Pr	Prandtl number
H	heat generation parameter
ϵ_2, ϵ_1	very small parameters
γ	fluidic number
σ	electrical density
E	electric field value
T	temperature
θ	temperature
C	concentration
M	magnetic number
u, v, w	velocity component
ϵ_1	very small parameter
λ	time relaxation number
Sc	Schmidt number
ρ	density
Sr	Soret number
k	thermal conductivity
F_r	Forchheimer parameter
C_p	specific heat
K_c	chemical reaction
ν	kinematic viscosity
C_∞	ambient concentration
Y, X, Z	space coordinates
T_∞	ambient temperature
s_1, s_2, s_3, s_4	solid nanoparticles
Tri	tri-hybrid nanofluid
Re	Reynolds number
Nu	Nusselt number
η	independent variable
Tet	tetra-hybrid nanofluid
hy	hybrid nanofluid
Nf	nanofluid
G	gravitational acceleration
K_M	thermal diffusion
X_1, X_2, X_3, X_4	volume fraction of nanoparticles
Γ	relaxation number

law, including a chemical reaction and study of thermal features in Williamson fluid by inserting hybrid nanoparticles. Zehra et al. [15] modeled the energy transfer structure in the presence of non-Fourier's theory over a curved surface in the occurrence of nanoparticles. Saleem et al. [16] formulated an energy transfer model based on non-Fourier's approach in Maxwell liquid. Asjad et al. [17] studied non-Newtonian fluid with hybrid nanoparticles in a convective channel using Prabhakar's fractional derivative.

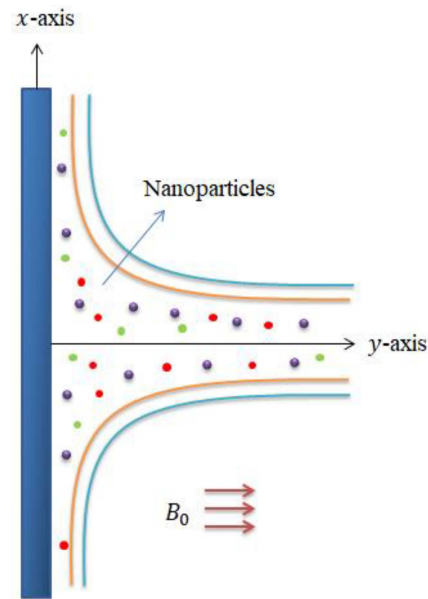


Fig. 1. The physical configuration of the model.

From published works, it is shown that a 2D-developed model in Reiner–Philippoff material, which passes through a porous perpendicular surface along a heat source and chemical reaction, has not been studied so far. Moreover, the variable mass transfer and heat conductivity are taken into account to explore the energy and mass transport models. Finally, the solution of the elaborated formulation is obtained numerically with the help of the finite element technique.

The structure of the paper is as follows. The literature review is covered in Sect. 1. The evolution of the model is defined in Sect. 2. In the third part, we discuss the finite element approach. Section 4 includes an analysis of graphical results, whereas Sect. 5 reveals the primary outcomes and results of the problem.

2. Mathematical analysis

Let us consider a mathematical analysis of Reiner–Philippoff material in which three different types of nanoparticles are suspended past a heated vertical sheet. A non-constant magnetic field is assumed in order to analyze thermal transfer and velocity field characterizations. At the same time, the chemical ratio is added to mass diffusion with the introduction of non-Fourier's law. Heat production and absorption terms are taken into account using non-Fourier's law and Darcy–Forchheimer theory [18, 19]. The nomenclature used in this paper is provided in Table I. Variable thermal properties of fluids are based on variable thermal conductivity. The thermal characteristics of tri-hybrid nanomaterials, hybrid nanomaterials, and nanoparticles are illustrated in Table II [20]. The physical diagram

TABLE II

Thermal properties of titanium dioxide, silicon dioxide, and aluminum oxide with engine oil [20].

	K [W/(m K)]	σ [S/m]	ρ [kg/m ³]
engine oil	0.144	0.125×10^{-11}	884
aluminium oxide	32.9	5.96×10^7	6310
titanium dioxide	8.953	2.4×10^6	4250
silicon dioxide	1.4013	3.5×10^6	2270
Cu	401	8933	59.5×10^6

of the analyzed system is presented in Fig. 1. The steady flow of Reiner–Philippoff martial is described by the partial differential equations (PDEs) and is built using boundary layer approximation, as displayed accordingly

$$\frac{\partial v_1}{\partial x} + \frac{\partial v_2}{\partial y} = 0, \quad (1)$$

$$v_1 \frac{\partial v_1}{\partial x} + v_2 \frac{\partial v_1}{\partial y} + \frac{\nu_{Tet}}{k^*} f v_1 = \frac{1}{\rho_{Tet}} \frac{\partial \tau}{\partial y} - \frac{B_0^2(x)}{\rho_{Tet}} v_1 - G\beta_1(T-T_\infty) - \frac{f}{(k^*)^{12}} v_1^2 - G\beta_2(C-C_\infty), \quad (2)$$

$$v_1 \frac{\partial T}{\partial x} + v_2 \frac{\partial T}{\partial y} + \gamma_1 \left[v_1^2 \frac{\partial^2 T}{\partial x^2} + v_2^2 \frac{\partial^2 T}{\partial y^2} + 2v_1 v_2 \frac{\partial^2 T}{\partial x \partial y} + \left(v_1 \frac{\partial v_1}{\partial x} + v_2 \frac{\partial v_1}{\partial y} \right) \frac{\partial T}{\partial x} + \left(v_2 \frac{\partial v_2}{\partial x} + v_1 \frac{\partial v_2}{\partial y} \right) \frac{\partial T}{\partial y} - \frac{Q_0}{(\rho C_p)_{Tet}} \left(v_1 \frac{\partial T}{\partial x} + v_2 \frac{\partial T}{\partial y} \right) \right] = \frac{1}{(\rho C_p)_{Tet}} \frac{\partial}{\partial y} \left(k_{Tet}^T \frac{\partial T}{\partial y} \right) - \frac{Q_0}{(\rho C_p)_{Tet}} (T-T_\infty), \quad (3)$$

$$v_1 \frac{\partial C}{\partial x} + v_2 \frac{\partial C}{\partial y} + \gamma_1 \left[v_1^2 \frac{\partial^2 C}{\partial x^2} + v_2^2 \frac{\partial^2 C}{\partial y^2} + 2v_1 v_2 \frac{\partial^2 C}{\partial x \partial y} + \left(v_2 \frac{\partial v_1}{\partial x} + v_1 \frac{\partial v_1}{\partial y} \right) \frac{\partial C}{\partial x} + \left(v_2 \frac{\partial v_2}{\partial x} + v_1 \frac{\partial v_2}{\partial y} \right) \frac{\partial C}{\partial y} - K_M \left(v_2 \frac{\partial C}{\partial y} + v_1 \frac{\partial C}{\partial x} \right) \right] = K_M (C-C_\infty) + \frac{\partial}{\partial y} \left(D_{Tet} \frac{\partial C}{\partial y} \right). \quad (4)$$

These equations ((1)–(4)) are subjected to desired boundary conditions

$$\begin{cases} \dot{v}_1 = ax^{\frac{1}{3}}, C = C_w, v_2 = 0, T = T_w, y \rightarrow 0, \\ C \rightarrow C_\infty, v_1 \rightarrow 0, T \rightarrow T_\infty, y \rightarrow \infty. \end{cases} \quad (5)$$

Similarly, variables and concentrations that change with temperature and thermal conductivity can be described as

$$\eta = y \sqrt{\frac{a}{\nu_f}}, \quad \psi = x^{\frac{2}{3}} \sqrt{a\nu_f}, \quad \tau = \rho_f x^{\frac{2}{3}} \sqrt{a^3 \nu_f}, \quad (6)$$

$$T = \frac{T-T_w}{T_w-T_\infty}, \quad C = \frac{C-C_w}{C_w-C_\infty}, \quad (7)$$

$$k_{Tet}^t = k_{hy} \left[1 + \epsilon_1 \left(\frac{T-T_\infty}{T_w-T_\infty} \right) \right], \quad (8)$$

$$D_{Tet}^c = D_{hy} \left[1 + \epsilon_2 \left(\frac{T-T_\infty}{T_w-T_\infty} \right) \right]. \quad (9)$$

Next, the system of dimensionless ordinary differential equations (ODEs) is formulated as

$$D_1 G - F'' \frac{G^2 + \lambda r^2}{G^2 + r^2} = 0, \quad (10)$$

$$G' - D_1 \frac{1}{3} F'^2 + D_1 \frac{2}{3} F F'' - \frac{\sigma_{Tet}}{\sigma_f} M F' + D_1 \lambda_1 \theta - \epsilon F' - D_1 F_r F'^2 + D_1 \lambda_2 \varphi = 0, \quad (11)$$

$$(1 + \epsilon_1 \theta) \theta'' + \epsilon_1 (\theta')^2 + Pr \Gamma \frac{k_f (\rho C_p)_{Tet}}{k_{Tet} (\rho C_p)_f} \left[F F' \theta' + \eta F^2 \theta'' + H F \theta' \right] + \frac{k_f (\rho C_p)_{Tet}}{k_{Tet} (\rho C_p)_f} \frac{2}{3} Pr F \theta' + \frac{k_f}{k_{Tet}} H Pr \theta = 0, \quad (12)$$

$$(1 + \epsilon_1 \varphi) \varphi'' + \epsilon_2 \varphi' \theta' + \frac{2}{3} Pr F \varphi' + \frac{Sc \Gamma_1}{D_2} \left[F F' \varphi' + \eta F^2 \varphi'' + K_c F \varphi' \right] - \frac{K_c Sc}{D_2} \varphi = 0. \quad (13)$$

The corresponding boundary conditions are expressed as

$$\begin{aligned} F'(0) = 1, \quad F(0) = 0, \quad \varphi(0) = 0, \quad \theta(0) = 0, \\ F(\infty) \rightarrow 0, \quad \varphi(\infty) \rightarrow 0, \quad \theta(\infty) \rightarrow 0. \end{aligned} \quad (14)$$

Hence, we introduce the following nomenclature. A composite relation of copper, silicon dioxide, aluminum oxide, and titanium dioxide with engine oil is called a tetra-hybrid nanofluid; a composite relation of copper, silicon dioxide, and aluminum oxide with engine oil is termed a tri-hybrid nanofluid; a composite relation of copper and silicon dioxide is known as a hybrid nanofluid; and copper is called a nanofluid (see Table II). The connections among fluid, nanofluid, tri-hybrid nanofluid, tetra-hybrid nanofluid, hybrid nanofluid, and base fluid are the correlations associated with tetra-hybrid nanostructures. They are defined as

$$\mu_{Tet} = \frac{\mu_f}{(1-X_1)^{2.5} (1-X_2)^{2.5} (1-X_3)^{2.5} (1-X_4)^{2.5}}, \quad (15)$$

$$\rho_{\text{Tet}} = (1-X_4) \left\{ (1-X_3)(1-X_2) \left[(1-X_1) + \frac{X_1 \rho_{s1}}{\rho_f} \right] + \frac{X_2 \rho_{s2}}{\rho_f} + \frac{X_3 \rho_{s2}}{\rho_f} + \frac{X_4 \rho_{s2}}{\rho_f} \right\}, \quad (16)$$

$$(\rho C_p)_{\text{Tet}} = (1-X_1)(1-X_2)(1-X_3)(1-X_4) \times \left((1-X_1) + \frac{X_1 (\rho C_p)_{s1}}{(\rho C_p)_f} \right) + \frac{X_2 (\rho C_p)_{s2}}{(\rho C_p)_f} + \frac{X_3 (\rho C_p)_{s3}}{(\rho C_p)_f} + \frac{X_4 (\rho C_p)_{s4}}{(\rho C_p)_f}, \quad (17)$$

$$\frac{k_{\text{Tet}}}{k_f} = \frac{k_{s4} + 2k_{\text{Tri}} - 2X_4 (k_{\text{Tri}} - k_{s4})}{k_{s4} + 2k_{\text{Tri}} + X_4 (k_{\text{Tri}} - k_{s4})}, \quad (18)$$

$$\frac{k_{\text{Tri}}}{k_f} = \frac{k_{s3} + 2k_{\text{hy}} - 2X_3 (k_{\text{hy}} - k_{s3})}{k_{s3} + 2k_{\text{hy}} + X_3 (k_{\text{hy}} - k_{s3})}, \quad (19)$$

$$\frac{k_{\text{hy}}}{k_f} = \frac{k_{s2} + 2k_{\text{Nf}} - 2X_2 (k_{\text{Nf}} - k_{s2})}{k_{s2} + 2k_{\text{Nf}} + X_2 (k_{\text{Nf}} - k_{s2})}, \quad (20)$$

$$\frac{k_{\text{Nf}}}{k_f} = \frac{k_{s1} + 2k_f - 2X_1 (k_f - k_{s1})}{k_{s1} + 2k_{\text{hy}} + X_1 (k_f - k_{s1})}, \quad (21)$$

$$\frac{\sigma_{\text{Tet}}}{\sigma_f} = \frac{\sigma_{s4} + 2\sigma_{\text{Tri}} - 2X_4 (\sigma_{\text{Tri}} - \sigma_{s4})}{\sigma_{s4} + 2\sigma_{\text{Tri}} + 2X_4 (\sigma_{\text{Tri}} - \sigma_{s4})}, \quad (22)$$

$$\frac{\sigma_{\text{Tri}}}{\sigma_f} = \frac{\sigma_{s3} + 2\sigma_{\text{hy}} - 2X_3 (\sigma_{\text{hy}} - \sigma_{s3})}{\sigma_{s3} + 2\sigma_{\text{hy}} + 2X_3 (\sigma_{\text{hy}} - \sigma_{s3})}, \quad (23)$$

$$\frac{\sigma_{\text{hy}}}{\sigma_f} = \frac{\sigma_{s2} + 2\sigma_{\text{Nf}} - 2X_2 (\sigma_{\text{Nf}} - \sigma_{s2})}{\sigma_{s2} + 2\sigma_{\text{Nf}} + 2X_2 (\sigma_{\text{Nf}} - \sigma_{s2})}, \quad (24)$$

$$\frac{\sigma_{\text{Nf}}}{\sigma_f} = \frac{\sigma_{s1} + 2\sigma_f - 2X_1 (\sigma_f - \sigma_{s1})}{\sigma_{s1} + 2\sigma_f + 2X_1 (\sigma_f - \sigma_{s1})}, \quad (25)$$

$$\frac{k_{\text{Tet}}}{k_f} = \frac{k_{s4} + 2k_{\text{Tri}} - 2X_4 (k_{\text{Tri}} - k_{s4})}{k_{s4} + 2k_{\text{Tri}} + X_4 (k_{\text{Tri}} - k_{s4})} \times \frac{k_{s3} + 2k_{\text{hy}} - 2X_3 (k_{\text{hy}} - k_{s3})}{k_{s3} + 2k_{\text{hy}} + X_3 (k_{\text{hy}} - k_{s3})} \times \frac{k_{s2} + 2k_{\text{hy}} - 2X_2 (k_{\text{Nf}} - k_{s2})}{k_{s2} + 2k_{\text{hy}} + X_2 (k_{\text{hy}} - k_{s2})} \times \frac{k_{s1} + 2k_f - 2X_1 (k_{\text{Nf}} - k_{s1})}{k_{s1} + 2k_f + X_1 (k_f - k_{s1})}, \quad (26)$$

$$\frac{k_{\text{Tet}}}{k_f} = \frac{\sigma_{s4} + 2\sigma_{\text{Tri}} - 2X_4 (\sigma_{\text{Tri}} - \sigma_{s4})}{\sigma_{s3} + 2\sigma_{\text{Tri}} + X_4 (\sigma_{\text{Tri}} - \sigma_{s4})} \times \frac{\sigma_{s3} + 2\sigma_{\text{hy}} - 2X_3 (\sigma_{\text{hy}} - \sigma_{s3})}{\sigma_{s3} + 2\sigma_{\text{hy}} + X_3 (\sigma_{\text{hy}} - \sigma_{s3})} \times \frac{\sigma_{s2} + 2\sigma_{\text{Nf}} - 2X_2 (\sigma_{\text{Nf}} - \sigma_{s2})}{\sigma_{s3} + 2\sigma_{\text{Nf}} + X_3 (\sigma_{\text{Nf}} - \sigma_{s3})} \times \frac{\sigma_{s1} + 2\sigma_f - 2X_1 (\sigma_f - \sigma_{s1})}{\sigma_{s1} + 2\sigma_f + X_1 (\sigma_f - \sigma_{s1})}, \quad (27)$$

$$D_2 = \frac{1}{(1-X_1)^{2.5} (1-X_2)^{2.5} (1-X_3)^{2.5} (1-X_4)^{2.5}}. \quad (28)$$

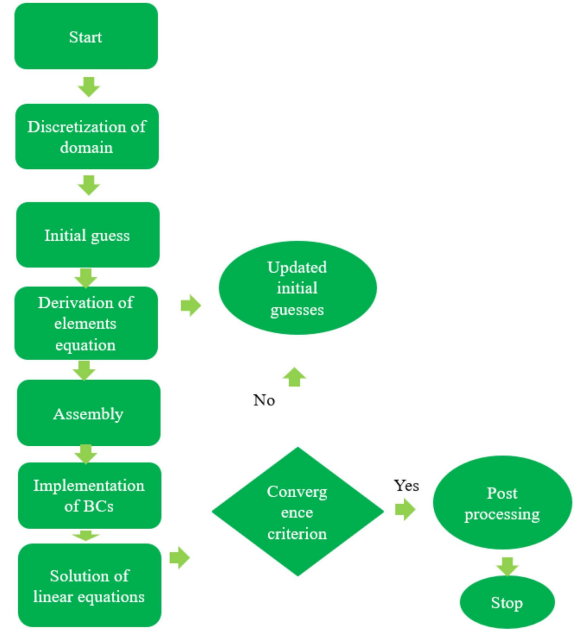


Fig. 2. The flowchart of the finite element method.

The value of thermal energy transfer and the value of mass transfer are obtained, respectively, as

$$Nu = \frac{-xk_{\text{hy}} \left(\frac{\partial T}{\partial y} \Big|_{y=0} \right)}{(T_w - T_\infty)k_f} \frac{Nu}{\sqrt{Re}} = -\frac{k_{\text{hy}}}{k_f} \theta'(0), \quad (29)$$

and

$$Sh = \frac{-xQ_t}{D(C - C_\infty)} = \frac{Sh}{\sqrt{Re}} = -\frac{1}{D_2} \phi'(0), \quad (30)$$

where $Re (= U_w x / \nu_f)$ is a dimensionless number, known as a Reynolds number, and it describes flow behavior.

3. Numerical solution

The finite element technique is used to solve a set of dimensionless, non-linear ordinary differential equations (ODEs) defined in Sect. 2. The procedure regarding computation is discussed below.

Step 1: A system of ordinary differential equations (ODEs) is expressed in terms of residuals, and weighted integral residuals are used to construct weak forms.

Step 2: The element's stiffness matrixes are obtained using the Galerkin approach. Due to the non-linearity of the present problem, variable nodal values are associated with the matrix related to global stiffness. Additionally, non-linear algebraic equations are converted into linear equations using Picard's technique.

Step 3: Under the computational tolerance of an iterative simulation, the system of algebraic equations is completed.

Step 4: The results of the calculations are displayed in tables and graphs.

TABLE III

Comparison of results with published work [21], when $X_1 = X_2 = X_3 = X_4 = 0, M = 0$.

γ	Sajid et al. [21] (shooting approach)	Present work (finite element method)
0.1	0.130909	0.132903690243
0.2	0.109284	0.109033421081
0.3	0.085161	0.109032201540

TABLE IV

Velocity, temperature, and concentration profiles vs number of finite elements.

No. of elements	$F'(\frac{\eta_{max}}{2})$	$\theta(\frac{\eta_{max}}{2})$	$\varphi(\frac{\eta_{max}}{2})$
30	0.03739643693	0.007435435051	0.009773428084
60	0.03652941667	0.003617569756	0.004548750392
90	0.03623026090	0.002433140864	0.002959697248
120	0.03607872439	0.001849791306	0.002192563678
150	0.03598713063	0.001500248584	0.001740935198
180	0.03592576537	0.001266406353	0.001443441685
210	0.03588178671	0.001098466029	0.001232702583
240	0.03584874587	0.0009717300891	0.001075606893
270	0.03582297916	0.0008725175218	0.0009539964889
300	0.03580234563	0.0007926265239	0.0008570696942

Step 5: The finite element approach for a modeled problem is achieved using the indigenous Maple code. A mesh-free analysis is conducted for the computational domain $[0, 8]$, which is mentioned in Table III.

Step 6: This phase has to do with solving algebraic problems. Various different numbers of elements simulate and carry out the solution of algebraic equations. Table III describes the validation of numerical results compared to the published study [21]. Table IV presents a mesh-free study for 300 elements. Moreover, Table IV describes convergence analysis. The flow chart of required FEM is shown in Fig. 2.

4. Results and analysis

Reiner–Philippoff martial in the view of the vertical plane influences the development of a two-dimensional model. Energy transfer and transportation of mass species are carried out in the presence of non-Fourier’s law, which is combined with chemical reaction parameters and thermal sources, considering tetra-hybrid nanoparticles. The concentration and energy equations are inserted into the mass diffusion and thermal conductivity variables. Numerical studies of the present model have been performed with the finite element method. Below, we present graphical descriptions of flow, thermal energy, and concentration versus different parameters.

4.1. A study of the motion of fluid

Figures 3–6 display velocity curves against a heat source, fluid, and magnetic parameters. The analysis of the effects of tri-hybrid nanoparticles, tetra-hybrid nanofluids, and nanofluids on the velocity field is carried out versus the fundamental parameters and shown in Figs. 3–6. It is observed that dash-dotted lines depict tri-hybrid nanoparticle behavior, while dotted curves represent the position of tetra-hybrid nanoparticles. The impact of H on velocity curve has been predicted.

Figure 4 has been created to visually represent the characteristics of the heat-generating component in the fluidic motion. It has been found that increasing the number of heat sources leads to increased fluid mobility. Physically, the outer heat source is applied to the surface’s wall to control the distribution of heat energy into particles. The

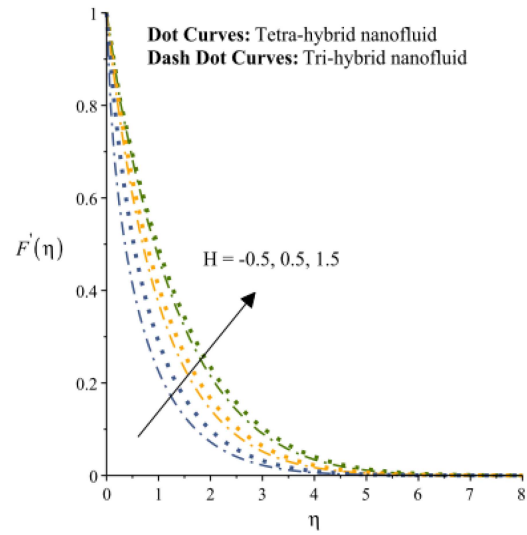


Fig. 3. The influence of H on the velocity v .

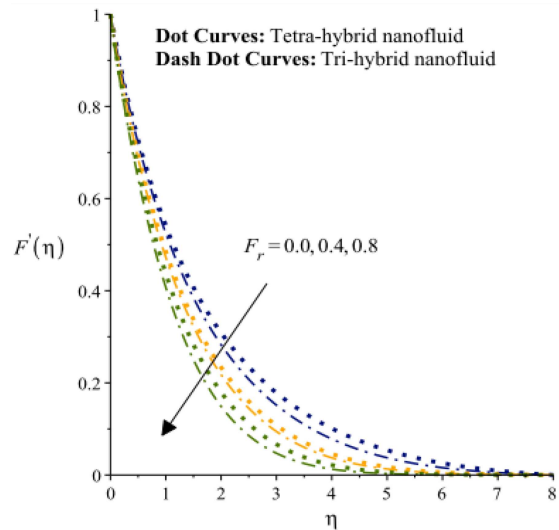


Fig. 4. The influence of F_r on the velocity v .

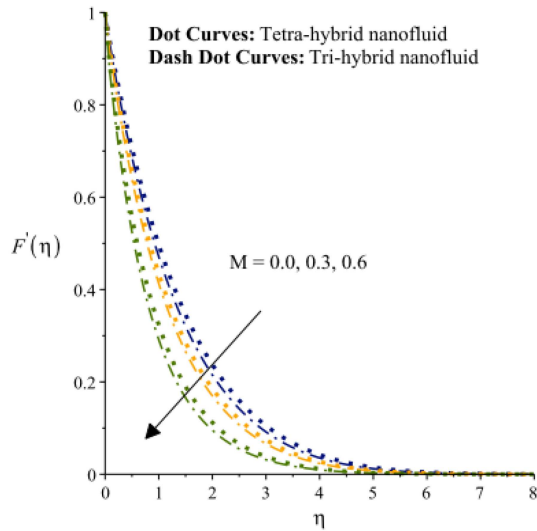


Fig. 5. The influence of M on the velocity v .

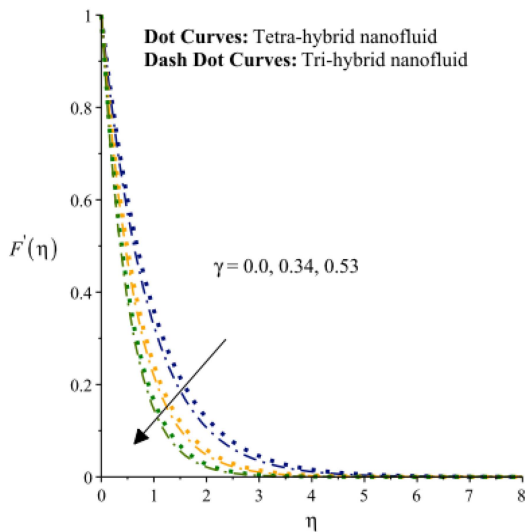


Fig. 6. The influence of γ on the velocity v .

phenomenon of heat generation is observed when the heat source parameter exhibits positive values, whereas heat absorption occurs when the heat source parameter exhibits negative values. The effect of this on fluid motion is predicted in Fig. 5. The momentum boundary layers depend on the fluctuations of F_r . It is stated that fluidic particles experience resistance due to a retardation motion that is formed in motion concerning particles. Momentum boundary layers decline when increasing the values of F_r . A large number of pores are precisely placed on the surface. As a result, a rise in F_r reduces the velocity field. It is observed that the motion of fluid for tetra-hybrid nanofluid is greater than the motion of fluid for the case of tri-hybrid nanoparticles. Moreover, Fig. 5 shows how magnetic parameters change velocity curves, specifically for a mixture of three different kinds of nanoparticles. It is seen that the magnetic parameter is a key factor

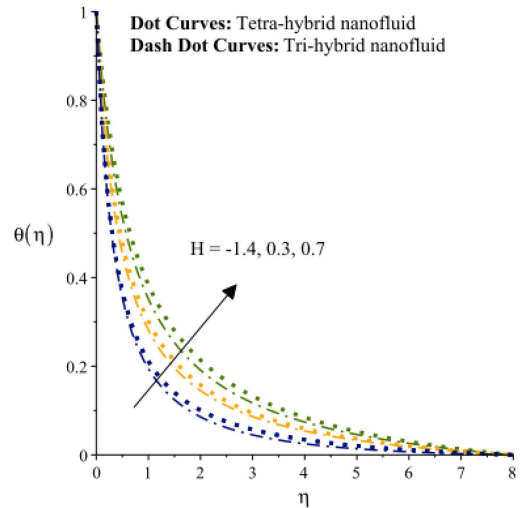


Fig. 7. The influence of H_t on the thermal energy curve.

in reducing the velocity of fluidic particles. Because Lorentz's force, which is supposed to be negative, is applied in the moment equation, this opposing force creates resistance in fluidic particles. Because Lorentz's force, which is supposed to be negative, is applied in the moment equation, this opposing force creates resistance in fluidic particles. Figure 6 is plotted to determine the effect on the velocity field. This dimensionless parameter is described as a result of the Reiner–Philippoff liquid's presence in the momentum equation. It is noticed that the motion of the fluid declines when γ is increased. Furthermore, thickness based on momentum boundary layers is declined using a higher impact of γ . This graph indicates that the fluidic motion of tetra-hybrid nanoparticles is much more heightened than the fluidic motion of tri-hybrid nanoparticles.

4.2. A study of fluidic temperature

The results in Figs. 7–9 show the impact of fluidic temperature as opposed to changes in the variable thermal conductivity number and heat source parameter. It is mentioned that tetra-hybrid nanofluids are depicted using dotted lines, but tri-hybrid nanofluids are analyzed using dash–dotted lines. Figure 7 has been created to illustrate the relationship between heat source parameters and fluidic temperature. The fluidic temperature increases when an external heat source is applied to the wall. In general, positive values of the heat source parameter are indicative of heat production, whereas negative values indicate heat absorption. Thus, thermal layer thickness is increased over heat source parameter values.

The character of ϵ_1 on thermal layers is illustrated in Fig. 8. It is noticed that the appearance of ϵ_1 is created due to the involvement of variable thermal conductivity numbers. The current study

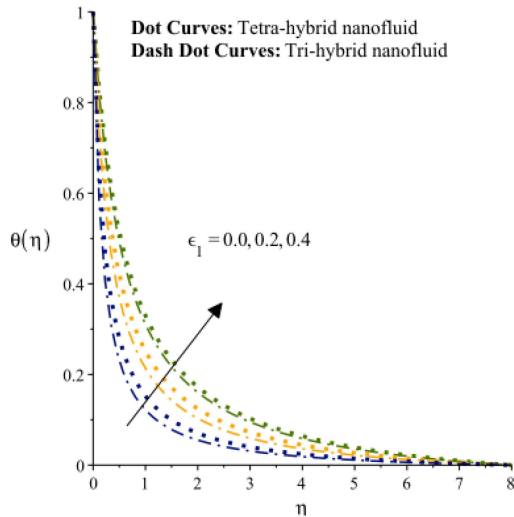


Fig. 8. The influence of ϵ_1 on the thermal energy curve.

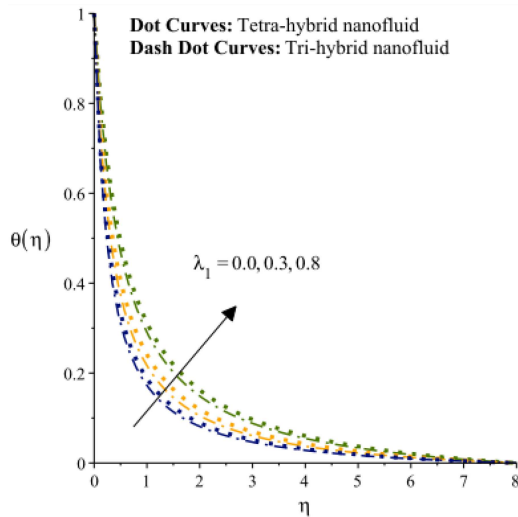


Fig. 9. The influence of λ_1 on the thermal energy curve.

considers the thermal conductivity in terms of the thermal energy. In mathematical terms, thermal conductivity depends on temperature, while ϵ_1 depends on the temperature difference. Thus, increasing ϵ_1 increases temperature difference. Furthermore, the fluidic temperature in the case of ternary tri-hybrid nanoparticles is observed to be higher than the fluidic temperature in the case of tri-hybrid nanoparticles.

Figure 9 shows the influence of thermal energy versus the behavior of the time relaxation number. It has been analyzed that the involvement of the time relaxation parameter is introduced as a consequence of the presence of the time relaxation number. Moreover, non-Fourier methods are employed to analyze concentration and energy equations. The capability of fluid temperature is improved by employing a relaxation time parameter.

4.3. An investigation of fluidic concentration

Figures 10, 11 and 12, are created to determine the characterization concentration of fluid against the effect of Sc , K_c , and time relaxation parameters by inserting a tetra-hybrid nanofluid. The dotted lines depict the characteristics of a tetra-hybrid nanofluid, while dash-dotted lines depict those of a tri-hybrid nanofluid. The effect of Sc on fluidic concentration when tri-hybrid and tetra-hybrid nanofluids are present is shown in Fig. 10. Physically, it is the ratio of momentum and mass diffusion diffusivities. As a result, an inversely proportional relationship occurs versus the effect of the Schmidt number. So, an increase in Sc results in an increase in mass diffusivity.

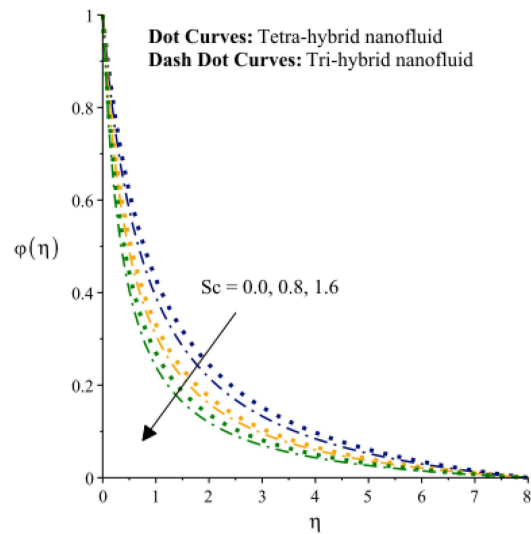


Fig. 10. The influence of Sc on the concentration curves.

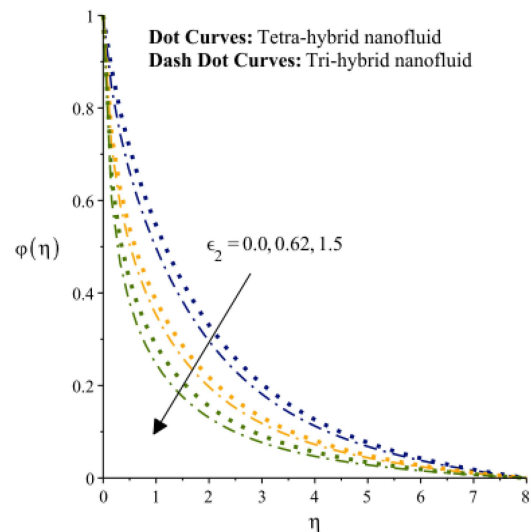


Fig. 11. The influence of ϵ_2 on the concentration profile.

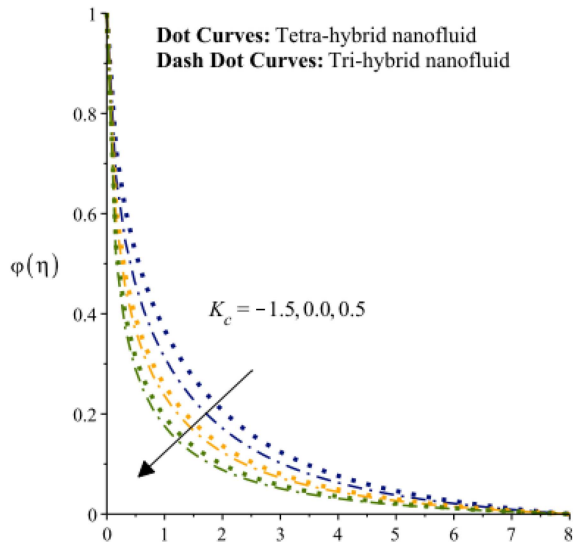


Fig. 12. The influence of K_c on the concentration curves.

Moreover, mass diffusion for tetra-hybrid nanofluid is more elevated than the quantity of mass diffusion in the case of hybrid nanostructures. The connection between mass diffusion and the variable mass diffusion number is depicted in Fig. 11. It can be seen that the effect of variable mass diffusion causes the rise of mass diffusion. Furthermore, variable mass diffusion is also temperature-dependent. Thus, mass diffusion declines when ϵ_2 is increased. Figure 12 shows the effect of a chemical reaction's parameter on mass diffusion. When the chemical reaction parameter is either positive or negative, two distinct types of reactions occur. In both circumstances, a higher K_c results in less mass diffusion.

5. Conclusions

A two-dimensional model based on non-Fourier's law implements fluidic features such as velocity, thermal energy, and concentration. Tetra-hybrid nanofluids introduce both temperature-dependent mass diffusion and temperature-dependent thermal conductivity. Thermal sources and chemical reactions are also taken into account. A finite element approach is used to obtain the numerical solution. The main observations are summarized below.

- Fluidic motion is boosted versus numerical values for the argument heat source parameter, but fluidic motion slows down against more significant numbers for the magnetic parameter and the Forchheimer parameter.
- The thermal energy of the fluid is increased as opposed to a higher rate of heat source number, variable thermal conductivity parameter, and time relaxation number.

- The concentration of fluid declines as opposed to the change in chemical reaction parameters and Schmidt number.
- The fluidic temperature of the tetra-hybrid nanofluid case exhibits higher values compared to the fluidic temperature of the tri-hybrid nanofluid case. This trend is also observed in the fluidic temperature and fluidic concentration analyses.

References

- [1] A. Ali, S. Saleem, S. Mumraiz, A. Saleem, M. Awais, D.N. Khan Marwat, *J. Therm. Anal. Calorim.* **143**, 1985 (2021).
- [2] A. Ali, A. Noreen, S. Saleem, A.F. Aljohani, M. Awais, *J. Therm. Anal. Calorim.* **143**, 2367 (2021).
- [3] Z. Ahmed, S. Saleem, S. Nadeem, A.U. Khan, *Arab. J. Sci. Eng.* **46**, 2047 (2021).
- [4] D. Gopal, S. Saleem, S. Jagadha, F. Ahmad, A.O. Almatroud, N. Kishan, *Alex. Eng. J.* **60**, 1861 (2021).
- [5] A.S. Oke, I.L. Animasaun, W.N. Mutuku, M. Kimathi, N.A. Shah, S. Saleem, *Chinese J. Phys.* **71**, 716 (2021).
- [6] S. Saleem, B. Heidarshenas, *J. Therm. Anal. Calorim.* **45**, 1599 (2021).
- [7] T. Elnaqeeb, I.L. Animasaun, N.A. Shah, *Z. Naturforsch. A* **76**, 231 (2021).
- [8] E. Hou, F. Wang, U. Nazir, M. Sohail, N. Jabbar, P. Thounthong, *Micromachines* **13**, 201 (2022).
- [9] F. Wang, U. Nazir, M. Sohail, E.R. El-Zahar, C. Park, P. Thounthong, *Nanotechnol. Rev.* **11**, 834 (2022).
- [10] U. Nazir, M. Sohail, H. Alrabaiah, M.M. Selim, P. Thounthong, C. Park, *PLOS ONE* **16**, e0256302 (2021).
- [11] S. Manjunatha, V. Puneeth, B.J. Giresha, A. Chamkha, *J. Appl. Comput. Mech.* **8**, 1279 (2022).
- [12] H. Adun, D. Kavaz, M. Dagbasi, *J. Clean Prod.* **328**, 129525 (2021).
- [13] U. Nazir, S. Saleem, M. Nawaz, M.A. Sadiq, A.A. Alderremy, *Phys. A Statist. Mech. App.* **554**, 123921 (2020).
- [14] U. Nazir, M.A. Sadiq, M. Nawaz, *Int. Commun. Heat Mass Transf.* **127**, 105536 (2021).
- [15] I. Zehra, N. Abbas, M. Amjad, S. Nadeem, S. Saleem, A. Issakhov, *Case Studies Therm. Eng.* **27**, 101146 (2021).
- [16] M. Saleem, M.N. Tufail, *Indian J. Phys.* (2023).

- [17] M.I. Asjad, N. Sarwar, M.B. Hafeez, W. Sumelka, T. Muhammad, *Fractal Fract.* **5**, 99 (2021).
- [18] H. Darcy, *Les Fontaines Publiques De La Ville De Dijon*, Victor Dalmont, Paris 1856.
- [19] P. Forchheimer, *Z. Ver. D. Ing.* **45**, 1782 (1901).
- [20] M. Sohail, U. Nazir, A. Singh, A. Tulu, M.J. Khan, *Sci. Rep.* **14**, 1520 (2024).
- [21] T. Sajid, M. Sagheer, S. Hussain, *Math. Prob. Eng.* **2020**, 9701860 (2020).